Theory and Implementation of Fractional Order Controllers for Power System Applications

Georgios Tzounas, *Student Member, IEEE*, Ioannis Dassios,
Mohammed Ahsan Adib Murad, *Student Member, IEEE*, and Federico Milano, *Fellow, IEEE*

***Abstract*— The paper presents the theoretical foundation and practical implementation aspects of Fractional Order Controllers (FOCs) for power system applications. With this aim, the paper provides a comprehensive mathematical background on the stability analysis of dynamic systems with inclusion of fractional order derivatives and discusses their software implementation based on the Oustaloup's Recursive Approximation (ORA) method. Then the paper illustrates a variety of examples of ORA-based FOCs, namely, automatic generation control of synchronous machines; frequency control of a converter-interfaced energy storage system; and voltage control through a static synchronous compensator. The WSCC 9-bus test system and a realistic 1,479-bus model of the Irish transmission system are employed to test and compare the examined FOCs with their integer-order versions.**

***Index Terms*— Fractional Order Controllers (FOCs), power system stability, Oustaloup's Recursive Approximation (ORA), frequency regulation, voltage regulation.**

I. INTRODUCTION

A. Motivation

Control schemes based on fractional calculus have gained momentum in power system applications due to their ability to enhance performance and increase the stability margin, under the presence of topological changes, parameter uncertainty and noise. This paper provides an in-depth study on Fractional Order Controllers (FOCs) for power system applications.

B. Literature Review

Fractional calculus is the analysis of non-integer order differentials and integrals. Although the first discussion on derivatives with fractional order dates back to Leibniz [1], major studies on fractional calculus started with Liouville [2]. The application of fractional calculus in control was introduced with the definition of the ideal cutoff characteristic by Bode [3] and the first systematic study of the frequency response of FOCs was done by Oustaloup [4]. In [5] and [6], Podlunby proposed the Fractional Order PID (FOPID) controller and provided a comprehensive analysis of fractional systems with applications to automatic control, respectively. FOCs have been applied to various engineering fields, e.g. heat diffusion [7] and robotic time-delay systems [8].

The authors are with AMPSAS, School of Electrical and Electronic Engineering, University College Dublin, Ireland. E-mails: georgios.tzounas @ucdconnect.ie, ioannis.dassios@ucd.ie, mohammed.murad@ucdconnect.ie and federico.milano@ucd.ie.

This work is supported by the Science Foundation Ireland, by funding Georgios Tzounas, Ioannis Dassios, Mohammed Ahsan Adib Murad and Federico Milano, under Investigator Programme Grant No. SFI/15/IA/3074.

The potential of FOCs for power system applications has not been discussed until very recently. Applications include automatic voltage regulation of synchronous machines [9]–[11]; load frequency control [12], [13]; damping control [14]; and voltage control of distributed energy resource systems [15]. These works mainly focus on the tuning of FOPID controllers through heuristic algorithms, such as particle swarm [9], chaotic multi-objective [11], and imperialist competitive algorithm [12]. Analytical methods employ frequency response criteria such as the desired gain crossover frequency [13].

From a practical and simulation point of view, fractional dynamics are typically approximated using appropriate rational order transfer functions. Although various techniques have been proposed to define such transfer functions [16], the most commonly utilized continuous method is the Oustaloup's Recursive Approximation (ORA) [17]. Therefore, the ORA is the method considered in this paper. The works cited above focus on applications and rely, for the implementation of FOCs, on proprietary software tools which are utilized as a *black-box*. This approach is indeed fostered by the availability of several software tools for the design and simulation of FOCs. We cite, for example, the Matlab toolboxes CRONE [18], Ninteger [19], and FOMCON [20].

C. Contributions

The main goal of this paper is to provide a systematic study of FOCs for power system applications. The specific contributions of the paper are as follows:

- A theory on how to carry out small-signal stability analysis of power systems with *exact* fractional dynamics, as opposed to the approximated implementations that have been proposed in the literature.
- A step-by-step analytical study on the modelling and parameters selection of ORA-based FOCs, as opposed to standard approaches that are based on black-box applications of proprietary software tools for fractional dynamics.
- A systematic analysis of FOC applications to power system controllers. These include integral FOC for Automatic Generation Control (AGC); lead-lag FOC for frequency regulation of an Energy Storage System (ESS); and multiple PI FOCs for voltage regulation provided by a STATic synchronous COMpensator (STATCOM). The dynamic response of these controllers is compared with their conventional Integer Order (IO) versions.

Finally, the impact of FOC is evaluated in the context of a large-scale, realistic model of the all-island Irish transmission system.

D. Organization

The remainder of the paper is organized as follows. Section II outlines the theory of fractional calculus. Section III discusses the stability of power systems with inclusion of FOCs. Section IV focuses on the modelling, computer implementation and tuning of ORA-based FOCs. The case studies are presented in Sections V and VI. Conclusions are drawn in Section VII.

II. Essentials of Fractional Calculus

Fractional calculus deals with the problem of extending the differentiation and integration operators d^n/dt^n, $\int_0^t d^n(\tau)$, $n \in \mathbb{N}$, for real (or complex) number powers. There exist several approaches that address this problem.

A precise formulation of fractional calculus is given by the Riemann-Liouville (R-L) definition. Consider a function $\phi : [0, \infty) \to \mathbb{R}$. The idea behind the R-L definition is to first consider the n-fold integration of $\phi(t)$ and then extend $n \in \mathbb{N}$ to any $\gamma \in \mathbb{R}^+$. In its derivative form, the R-L definition reads [21]:

$$\phi^{(\gamma)}(t) = \frac{1}{\Gamma(\mu-\gamma)} \frac{d^\mu}{dt^\mu} \Big(\int_0^t \frac{\phi(\tau)}{(t-\tau)^{\gamma-\mu+1}} d\tau \Big) \ , \quad (1)$$

where γ, $\mu - 1 < \gamma < \mu$, $\mu \in \mathbb{N}$, is the fractional order; and $\phi^{(\gamma)}(t) = d^\gamma \phi / dt^\gamma$. The Laplace transform of (1) is:

$$\mathcal{L}\{\phi^{(\gamma)}(t)\} = s^\gamma \Phi(s) - \sum_{j=0}^{\mu-1} s^j \phi^{(\gamma-j-1)}(0) \ , \quad (2)$$

where $s \in \mathbb{C}$. Equation (2) requires the knowledge of the fractional order initial conditions $\phi^{(\gamma-j-1)}(0)$, $j = 0, 1, \ldots, \mu-1$. This raises an issue for engineering systems since, currently, only integer order initial conditions are well understood and known for physical variables. Other properties of the R-L definition are also counter-intuitive in the sense of classical differentiation. For example, the R-L derivative of a constant function is typically unbounded at $t = 0$ [5].

With the aim of meeting the requirements of known physical variables and systems, (1) was revisited by Caputo [22]. Caputo's definition of $\phi^{(\gamma)}(t)$ reads:

$$\phi^{(\gamma)}(t) = \frac{1}{\Gamma(\mu-\gamma)} \int_0^t \frac{\phi^{(\mu)}(\tau)}{(t-\tau)^{\gamma-\mu+1}} d\tau \ . \quad (3)$$

The Laplace transform of (3) is:

$$\mathcal{L}\{\phi^{(\gamma)}(t)\} = s^\gamma \Phi(s) - \sum_{j=0}^{\mu-1} s^{\gamma-j-1} \phi^{(j)}(0) \ . \quad (4)$$

Equation (4) requires the knowledge of the initial conditions $\phi^{(j)}(0)$, $j = 0, 1, \ldots, \mu - 1$, which in this case are of integer order. This property is crucial for the solution of initial value problems. In fact, for the purpose of fractional control, that is of concern here, one needs to use a definition with integer order initial conditions. However, in power system literature, many papers follow R-L and/or Grünwald-Letnikov definitions [9], [10], [14]. This work utilizes Caputo's definition of fractional derivative given in (3), which is more consistent for control applications and follows the properties of differentiation in the classical sense. For example, the Caputo's fractional derivative of a constant function is zero.

There are several other definitions of fractional derivatives/integrals and choosing the appropriate one depends on the application. For example, the Grünwald-Letnikov's derivative is relevant for the numerical solution of fractional differential equations. It is important to emphasize that the theory of fractional calculus applicable to the stability analysis and control of physical dynamical systems is an active research topic and yet to be fully understood. Recent efforts have addressed issues related to Caputo's formulation, for example its singular kernel for $t = \tau$ [22], [23].

III. Modelling and Stability of Power Systems with Inclusion of Fractional Derivatives

This section discusses the modelling and stability of power systems with inclusion of FOCs. Since a general theory of the stability of nonlinear fractional differential equations is not available, we proceed as follows. This section considers the conditions for the stability of linear (or linearized) fractional algebraic-differential equations. Such conditions help design the FOCs discussed in Section IV. However, power system models are non-linear. For this reason, we check the design of FOCs by solving numerical time domain simulations of the fully-fledged nonlinear model of the system and its controllers in the case studies presented in Sections V and VI.

A. Power System Model

The power system model for rotor angle and voltage stability studies consists of a set of non-linear Differential Algebraic Equations (DAEs), as follows:

$$\begin{aligned} \boldsymbol{x}'(t) &= \boldsymbol{f}(\boldsymbol{x}, \boldsymbol{y}, \boldsymbol{u}, t) \\ \boldsymbol{0}_{m,1} &= \boldsymbol{g}(\boldsymbol{x}, \boldsymbol{y}, \boldsymbol{u}, t) \ , \end{aligned} \quad (5)$$

where $\boldsymbol{f}$ ($\boldsymbol{f} : \mathbb{R}^{n+m+p} \to \mathbb{R}^n$), $\boldsymbol{g}$ ($\boldsymbol{g} : \mathbb{R}^{n+m+p} \to \mathbb{R}^m$) are the differential and algebraic equations; $\boldsymbol{x}$, $\boldsymbol{x} \in \mathbb{R}^n$, and $\boldsymbol{y}$, $\boldsymbol{y} \in \mathbb{R}^m$, are the state and algebraic variables, respectively; $\boldsymbol{u}$, $\boldsymbol{u} \in \mathbb{R}^p$, are controlled inputs; and $\boldsymbol{0}_{i,j}$, $\boldsymbol{0}_{i,j} \in \mathbb{R}^{i \times j}$, is the zero matrix. For sufficiently small disturbances, (5) can be linearized around an equilibrium point $(\boldsymbol{x}_0, \boldsymbol{y}_0, \boldsymbol{u}_0)$. In matrix form, the linearized system is as follows:

$$\begin{bmatrix} \boldsymbol{I}_n & \boldsymbol{0}_{n,m} \\ \boldsymbol{0}_{m,n} & \boldsymbol{0}_{m,m} \end{bmatrix} \begin{bmatrix} \Delta\boldsymbol{x} \\ \Delta\boldsymbol{y} \end{bmatrix}' = \begin{bmatrix} \boldsymbol{f}_x & \boldsymbol{f}_y \\ \boldsymbol{g}_x & \boldsymbol{g}_y \end{bmatrix} \begin{bmatrix} \Delta\boldsymbol{x} \\ \Delta\boldsymbol{y} \end{bmatrix} + \begin{bmatrix} \boldsymbol{f}_u \\ \boldsymbol{g}_u \end{bmatrix} \Delta\boldsymbol{u} \ ,$$

where $\Delta\boldsymbol{x} = \boldsymbol{x} - \boldsymbol{x}_0$, $\Delta\boldsymbol{y} = \boldsymbol{y} - \boldsymbol{y}_0$; $\Delta\boldsymbol{u} = \boldsymbol{u} - \boldsymbol{u}_0$; $\boldsymbol{f}_x$, $\boldsymbol{f}_y$, $\boldsymbol{f}_u$, $\boldsymbol{g}_x$, $\boldsymbol{g}_y$, $\boldsymbol{g}_u$, are the Jacobian matrices evaluated at $(\boldsymbol{x}_0, \boldsymbol{y}_0, \boldsymbol{u}_0)$. Using the notation

$$\boldsymbol{E} = \begin{bmatrix} \boldsymbol{I}_n & \boldsymbol{0}_{n,m} \\ \boldsymbol{0}_{m,n} & \boldsymbol{0}_{m,m} \end{bmatrix} \ , \ \boldsymbol{A} = \begin{bmatrix} \boldsymbol{f}_x & \boldsymbol{f}_y \\ \boldsymbol{g}_x & \boldsymbol{g}_y \end{bmatrix} \ , \ \boldsymbol{B} = \begin{bmatrix} \boldsymbol{f}_u \\ \boldsymbol{g}_u \end{bmatrix} \ ,$$

where $\boldsymbol{I}_n$, $\boldsymbol{I}_n \in \mathbb{R}^{n \times n}$, is the $n \times n$ identity matrix, we have

$$\boldsymbol{E}\Delta\hat{\boldsymbol{x}}' = \boldsymbol{A}\Delta\hat{\boldsymbol{x}} + \boldsymbol{B}\Delta\boldsymbol{u} \ , \quad (6)$$

where $\Delta\hat{\boldsymbol{x}} = [\Delta\boldsymbol{x} \;\; \Delta\boldsymbol{y}]^T$.

Let the vector of the system output measurements $\boldsymbol{w}$, $\boldsymbol{w} \in \mathbb{R}^{q\times 1}$, be:

$$\boldsymbol{w} = \boldsymbol{C}\Delta\hat{\boldsymbol{x}} + \boldsymbol{D}\Delta\boldsymbol{u} \ , \tag{7}$$

where $\boldsymbol{C} \in \mathbb{R}^{q\times(n+m)}$, $\boldsymbol{D} \in \mathbb{R}^{q\times p}$. Then, a Multiple-Input, Multiple-Output (MIMO) FOC for the system (6)-(7), can be described by a set of fractional DAEs as follows:

$$\begin{aligned} \boldsymbol{E}_c {\boldsymbol{x}_c}^{(\gamma)} &= \boldsymbol{A}_c\boldsymbol{x}_c + \boldsymbol{B}_c\boldsymbol{w} \ , \\ \boldsymbol{0}_{p,1} &= \boldsymbol{C}_c\boldsymbol{x}_c + \boldsymbol{D}_c\boldsymbol{w} - \Delta\boldsymbol{u} \ , \end{aligned} \tag{8}$$

where γ is the controller's fractional order; $\boldsymbol{x}_c$, $\boldsymbol{x}_c \in \mathbb{R}^{\nu}$, is the vector of the controller states; $\boldsymbol{E}_c$, $\boldsymbol{A}_c \in \mathbb{R}^{\nu\times\nu}$, $\boldsymbol{B}_c \in \mathbb{R}^{\nu\times q}$, $\boldsymbol{C}_c \in \mathbb{R}^{p\times\nu}$, $\boldsymbol{D}_c \in \mathbb{R}^{p\times q}$. It is relevant to mention that there are FOCs that introduce multiple, distinct fractional orders. Without loss of generality, we have chosen here to keep the analysis the simplest possible. Combining (6), (7) and (8) yields the closed-loop system representation. In matrix form:

$$\begin{bmatrix} \boldsymbol{E} & \boldsymbol{0}_{n,\nu} & \boldsymbol{0}_{n,p} \\ \boldsymbol{0}_{\nu,n} & \boldsymbol{0}_{\nu,\nu} & \boldsymbol{0}_{\nu,p} \\ \boldsymbol{0}_{p,n} & \boldsymbol{0}_{p,\nu} & \boldsymbol{0}_{p,p} \end{bmatrix} \begin{bmatrix} \Delta\hat{\boldsymbol{x}} \\ \boldsymbol{x}_c \\ \Delta\boldsymbol{u} \end{bmatrix}' + \begin{bmatrix} \boldsymbol{0}_{n,n} & \boldsymbol{0}_{n,\nu} & \boldsymbol{0}_{n,p} \\ \boldsymbol{0}_{\nu,n} & \boldsymbol{E}_c & \boldsymbol{0}_{\nu,p} \\ \boldsymbol{0}_{p,n} & \boldsymbol{0}_{p,\nu} & \boldsymbol{0}_{p,p} \end{bmatrix} \begin{bmatrix} \Delta\hat{\boldsymbol{x}} \\ \boldsymbol{x}_c \\ \Delta\boldsymbol{u} \end{bmatrix}^{(\gamma)}$$
$$= \begin{bmatrix} \boldsymbol{A} & \boldsymbol{0}_{n,\nu} & \boldsymbol{B} \\ \boldsymbol{B}_c\boldsymbol{C} & \boldsymbol{A}_c & \boldsymbol{B}_c\boldsymbol{D} \\ \boldsymbol{D}_c\boldsymbol{C} & \boldsymbol{C}_c & \boldsymbol{D}_c\boldsymbol{D} - \boldsymbol{I}_p \end{bmatrix} \begin{bmatrix} \Delta\hat{\boldsymbol{x}} \\ \boldsymbol{x}_c \\ \Delta\boldsymbol{u} \end{bmatrix} \ ,$$

or,

$$\boldsymbol{M}\boldsymbol{\xi}' + \boldsymbol{M}_\gamma\boldsymbol{\xi}^{(\gamma)} = \boldsymbol{A}_{cl}\boldsymbol{\xi} \ , \tag{9}$$

where $\boldsymbol{\xi} = [\Delta\hat{\boldsymbol{x}} \;\; \boldsymbol{x}_c \;\; \Delta\boldsymbol{u}]^T$, and

$$\boldsymbol{M} = \begin{bmatrix} \boldsymbol{E} & \boldsymbol{0}_{n,\nu} & \boldsymbol{0}_{n,p} \\ \boldsymbol{0}_{\nu,n} & \boldsymbol{0}_{\nu,\nu} & \boldsymbol{0}_{\nu,p} \\ \boldsymbol{0}_{p,n} & \boldsymbol{0}_{p,\nu} & \boldsymbol{0}_{p,p} \end{bmatrix} \ , \ \boldsymbol{M}_\gamma = \begin{bmatrix} \boldsymbol{0}_{n,n} & \boldsymbol{0}_{n,\nu} & \boldsymbol{0}_{n,p} \\ \boldsymbol{0}_{\nu,n} & \boldsymbol{E}_c & \boldsymbol{0}_{\nu,p} \\ \boldsymbol{0}_{p,n} & \boldsymbol{0}_{p,\nu} & \boldsymbol{0}_{p,p} \end{bmatrix} \ ,$$

$$\boldsymbol{A}_{cl} = \begin{bmatrix} \boldsymbol{A} & \boldsymbol{0}_{n,\nu} & \boldsymbol{B} \\ \boldsymbol{B}_c\boldsymbol{C} & \boldsymbol{A}_c & \boldsymbol{B}_c\boldsymbol{D} \\ \boldsymbol{D}_c\boldsymbol{C} & \boldsymbol{C}_c & \boldsymbol{D}_c\boldsymbol{D} - \boldsymbol{I}_p \end{bmatrix} \ .$$

B. Closed-loop System Stability

We study the stability of (9). With this aim, we first provide the following property of Caputo's fractional derivative [24]:

Proposition 1. Let $\boldsymbol{\phi}(t)$, $\boldsymbol{\phi}(t) \in \mathcal{C}^1[0,T]^{n\times 1}$ for some $T > 0$. Then:

$$[\boldsymbol{\phi}^{(a)}(t)]^{(b)} = [\boldsymbol{\phi}^{(b)}(t)]^{(a)} = \boldsymbol{\phi}^{(a+b)}(t) \ , \tag{10}$$

where $a, b \in \mathbb{R}^+$, and $a + b \leq 1$.

Note that (10) does not hold for the R-L derivative.

We rewrite (9) as:

$$\boldsymbol{M}\boldsymbol{\xi}^{(\gamma+\beta)} + \boldsymbol{M}_\gamma\boldsymbol{\xi}^{(\gamma)} = \boldsymbol{A}_{cl}\boldsymbol{\xi} \ , \tag{11}$$

where $\gamma + \beta = 1$. Adopting the notation:

$$\boldsymbol{\psi}_1 = \boldsymbol{\xi} \ , \ \boldsymbol{\psi}_2 = \boldsymbol{\xi}^{(\gamma)} \ ,$$

we obtain $\boldsymbol{\psi}_1^{(\gamma)} = \boldsymbol{\xi}^{(\gamma)} = \boldsymbol{\psi}_2$. Making use of (10), yields $\boldsymbol{\psi}_2^{(\beta)} = \boldsymbol{\xi}^{(\gamma+\beta)}$. Substitution to (11) gives:

$$\begin{aligned} \boldsymbol{M}\boldsymbol{\psi}_2^{(\beta)} + \boldsymbol{M}_\gamma\boldsymbol{\psi}_2 &= \boldsymbol{A}_{cl}\boldsymbol{\psi}_1 \ \Rightarrow \\ \boldsymbol{M}\boldsymbol{\psi}_2^{(\beta)} &= \boldsymbol{A}_{cl}\boldsymbol{\psi}_1 - \boldsymbol{M}_\gamma\boldsymbol{\psi}_2 \ . \end{aligned} \tag{12}$$

Equation (12) can be rewritten as:

$$\begin{bmatrix} \boldsymbol{I}_\rho & \boldsymbol{0}_{\rho,\rho} \\ \boldsymbol{0}_{\rho,\rho} & \boldsymbol{M} \end{bmatrix} \begin{bmatrix} \boldsymbol{\psi}_1^{(\gamma)} \\ \boldsymbol{\psi}_2^{(\beta)} \end{bmatrix} = \begin{bmatrix} \boldsymbol{0}_{\rho,\rho} & \boldsymbol{I}_\rho \\ \boldsymbol{A}_{cl} & -\boldsymbol{M}_\gamma \end{bmatrix} \begin{bmatrix} \boldsymbol{\psi}_1 \\ \boldsymbol{\psi}_2 \end{bmatrix} \ , \tag{13}$$

or, equivalently,

$$\tilde{\boldsymbol{M}}\boldsymbol{\psi}^{\Delta} = \tilde{\boldsymbol{A}}\boldsymbol{\psi} \ , \tag{14}$$

where

$$\tilde{\boldsymbol{M}} = \begin{bmatrix} \boldsymbol{I}_\rho & \boldsymbol{0}_{\rho,\rho} \\ \boldsymbol{0}_{\rho,\rho} & \boldsymbol{M} \end{bmatrix} \ , \ \tilde{\boldsymbol{A}} = \begin{bmatrix} \boldsymbol{0}_{\rho,\rho} & \boldsymbol{I}_\rho \\ \boldsymbol{A}_{cl} & -\boldsymbol{M}_\gamma \end{bmatrix} \ ,$$

$\rho = n + \nu + p$; $\boldsymbol{\psi} = [\boldsymbol{\psi}_1 \;\; \boldsymbol{\psi}_2]^T$; and $\boldsymbol{\psi}^{\Delta} = [\boldsymbol{\psi}_1^{(\gamma)} \;\; \boldsymbol{\psi}_2^{(\beta)}]^T$.

Theorem 1. Consider system (14). Then its matrix pencil is given by

$$\begin{bmatrix} s^\gamma\boldsymbol{I}_\rho & \boldsymbol{0}_{\rho,\rho} \\ \boldsymbol{0}_{\rho,\rho} & s^\beta\boldsymbol{I}_\rho \end{bmatrix} \tilde{\boldsymbol{M}} - \tilde{\boldsymbol{A}} \tag{15}$$

Proof. Let $\mathcal{L}\{\boldsymbol{\psi}(t)\} = \boldsymbol{\Psi}(s)$. Using Caputo's fractional derivative, by applying the Laplace transform $\mathcal{L}$ as defined in (4) for $\mu = 1$ into (14), we obtain

$$\tilde{\boldsymbol{M}}\mathcal{L}\{\boldsymbol{\psi}^{\Delta}(t)\} = \tilde{\boldsymbol{A}}\mathcal{L}\{\boldsymbol{\psi}(t)\},$$

Furthermore:

$$\tilde{\boldsymbol{M}}\mathcal{L}\Big\{ \begin{bmatrix} \boldsymbol{\psi}_1^{(\gamma)} \\ \boldsymbol{\psi}_2^{(\beta)} \end{bmatrix} \Big\} = \tilde{\boldsymbol{A}}\mathcal{L}\{\boldsymbol{\psi}(t)\} \ ,$$

or, equivalently,

$$\tilde{\boldsymbol{M}} \begin{bmatrix} s^\gamma\mathcal{L}\{\psi_1(t)\} - s^{\gamma-1}\psi_1(0) \\ s^\beta\mathcal{L}\{\psi_2(t)\} - s^{\beta-1}\psi_2(0) \end{bmatrix} = \tilde{\boldsymbol{A}}\mathcal{L}\{\boldsymbol{\psi}(t)\} \ ,$$

or, equivalently,

$$\tilde{\boldsymbol{M}} \begin{bmatrix} s^\gamma\mathcal{L}\{\psi_1(t)\} \\ s^\beta\mathcal{L}\{\psi_2(t)\} \end{bmatrix} - \tilde{\boldsymbol{M}} \begin{bmatrix} s^{\gamma-1}\psi_1(0) \\ s^{\beta-1}\psi_2(0) \end{bmatrix} = \tilde{\boldsymbol{A}}\mathcal{L}\{\boldsymbol{\psi}(t)\} \ ,$$

or, equivalently,

$$\tilde{\boldsymbol{M}} \begin{bmatrix} s^\gamma\boldsymbol{I}_\rho & \boldsymbol{0}_{\rho,\rho} \\ \boldsymbol{0}_{\rho,\rho} & s^\beta\boldsymbol{I}_\rho \end{bmatrix} \begin{bmatrix} \mathcal{L}\{\psi_1(t)\} \\ \mathcal{L}\{\psi_2(t)\} \end{bmatrix} -$$
$$\tilde{\boldsymbol{M}} \begin{bmatrix} s^{\gamma-1}\boldsymbol{I}_\rho & \boldsymbol{0}_{\rho,\rho} \\ \boldsymbol{0}_{\rho,\rho} & s^{\beta-1}\boldsymbol{I}_\rho \end{bmatrix} \begin{bmatrix} \psi_1(0) \\ \psi_2(0) \end{bmatrix} = \tilde{\boldsymbol{A}}\boldsymbol{\Psi}(s) \ ,$$

or, equivalently,

$$\Big(\tilde{\boldsymbol{M}} \begin{bmatrix} s^\gamma\boldsymbol{I}_\rho & \boldsymbol{0}_{\rho,\rho} \\ \boldsymbol{0}_{\rho,\rho} & s^\beta\boldsymbol{I}_\rho \end{bmatrix} - \tilde{\boldsymbol{A}}\Big)\boldsymbol{\Psi}(s) =$$
$$\begin{bmatrix} s^{\gamma-1}\boldsymbol{I}_\rho & \boldsymbol{0}_{\rho,\rho} \\ \boldsymbol{0}_{\rho,\rho} & s^{\beta-1}\boldsymbol{I}_\rho \end{bmatrix} \boldsymbol{\psi}(0) \ .$$

The proof is complete.

The eigenvalues of the matrix pencil (15) provide insight on

the stability of system (14), or equivalently, of system (9). We finally provide the following proposition, see [25]:

Proposition 2. Consider system (14). If $\tilde{\gamma} = \min\{\gamma, 1-\gamma\}$, and λ is an eigenvalue of the pencil (15), then system (14) is asymptotically stable if all eigenvalues λ satisfy:

$$|\mathrm{Arg}(\lambda)| > \tilde{\gamma}\frac{\pi}{2} \text{ (rad)} . \tag{16}$$

For linearized systems, as it is the case of power systems, the condition (16) guarantees stability in a neighborhood of the operating point utilized to calculate the pencil (15). For this reason, in the case studies discussed in Sections V and VI, we utilize numerical integration rather than (16) to check the stability and the dynamic response of power systems with inclusion of FOCs.

C. Illustrative Example

We provide an illustrative example on the small-signal stability analysis of power systems with inclusion of FOCs. The example is based on the well-known WSCC 9-bus system, the data of which are provided in [26]. The system consists of 3 synchronous machines, 6 transmission lines, 3 transformers and 3 loads, modelled as constant power consumption. Each machine provides primary voltage and frequency control through an Automatic Voltage Regulator (AVR) and a Turbine Governor (TG), respectively. The original system model does not include any fractional dynamics.

Suppose that a FO Power System Stabilizer (PSS) is installed at the synchronous machine connected at bus 2. The FO-PSS employed has the following transfer function:

$$G_{\mathrm{FOPSS}} = K\Big(\frac{T_1 s^\gamma + 1}{T_2 s^\gamma + 1}\Big)^2 ,$$

The controller input is the local rotor speed, while the output is an additional input to the algebraic equation of the local AVR reference. The FO-PSS can be written in the form of (8), where:

$$\boldsymbol{E}_c = \begin{bmatrix} T_2 & 0 & 0 & 0 \\ T_1 & 0 & 0 & 0 \\ 0 & 0 & T_2 & 0 \\ 0 & 0 & T_1 & 0 \end{bmatrix} , \ \boldsymbol{A}_c = \begin{bmatrix} -1 & 0 & 0 & 0 \\ -1 & 1 & 0 & 0 \\ 0 & 1 & -1 & 0 \\ 0 & 0 & -1 & 1 \end{bmatrix} ,$$

$$\boldsymbol{B}_c = \begin{bmatrix} K & 0 & 0 & 0 \end{bmatrix}^T , \ \boldsymbol{C}_c = \begin{bmatrix} 0 & 0 & 0 & 1 \end{bmatrix} , \ \boldsymbol{D}_c = 0.$$

Suppose that $T_1 = 0.01$ s, $T_2 = 0.22$ s, $\gamma = 0.75$. Then, small-signal stability is assessed by calculating the eigenvalues of (15). If λ_i is a finite eigenvalue and $\theta_i = \mathrm{Arg}(\lambda_\mathrm{i})$, then (16) suggests that the system is stable, if:

$$|\theta_i| > \tilde{\gamma}\frac{\pi}{2} = 0.393 \text{ rad} ,$$

where $\tilde{\gamma} = \min\{0.75, 0.25\} = 0.25$. The most critical eigenvalues of the closed-loop system are shown in Fig. 1, where the shaded region is unstable. As it can be seen, the system with the FO-PSS is in this case small-signal stable.

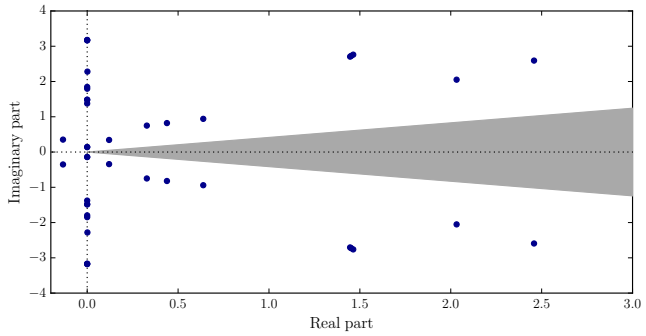

Fig. 1: WSCC system with FOPSS: most critical eigenvalues. Shaded is the region of instability.

D. Properties of FOCs

Let us consider the simple FOC with transfer function $G_c(s) = Ks^\gamma$. We consider the frequency response of $G_c(s)$, i.e. its steady-state response to sinusoidal, periodic input signals. In this case, it is $s \in \mathbb{I}$, or $s = j\omega$.

Frequency Response: The magnitude and phase of $G_c(s)$ can be written as follows:

$$\begin{aligned} \mathrm{Mag}(G_c(s)) \text{ (dB)} &= 20\log|Ks^\gamma| = 20\gamma\log(K\omega) , \\ \mathrm{Arg(G_c(s))} \text{ (}^\circ\text{)} &= \mathrm{Arg}(K(j\omega)^\gamma) = 90\gamma . \end{aligned} \tag{17}$$

Hence, $G_c(s)$ has a magnitude Bode plot with constant slope of 20γ dB/dec, while the phase plot is a horizontal line at 90γ degrees. The IO versions of $G_c(s)$ are obtained for $\gamma = n$, $n \in \mathbb{Z}$. Then, from (17), it is clear that $G_c(s)$ is an extension of its IO versions in frequency domain. This result is general, so that all FOCs can be viewed as extensions of the respective IO ones.

Robustness: FOCs have an inherent property of iso-damping, which implies that the closed-loop system is robust against gain uncertainties and variations. Let $P(s)$ be the transfer function of the open-loop, linearized power system. Then, the iso-damping property is defined as:

$$\left|\frac{\mathrm{Arg}(G_c(j\omega)P(j\omega))}{d\omega}\right|_{\omega=\omega_{\mathrm{gc}}} = 0 , \tag{18}$$

where ω_{gc} is the system gain crossover frequency. (18) indicates that the system maintains its phase margin around ω_{gc}.

IV. Oustaloup's Recursive Approximation

A. Formulation

The theoretical analysis based on fractional calculus is essential for a better understanding of "ideal" FOCs and hence, for a robust FOC design. In practice, however, the implementation of FOCs is typically done by approximating the fractional derivatives and integrals with rational transfer functions. Although this is an important aspect of FOCs implementation, some studies omit mentioning what approximation technique and/or parameters they use, effectively forcing the adoption of a black-box approach. In this paper, we employ the ORA method, that is arguably the most common continuous

approximation technique. The generalized ORA of a fractional derivative of order γ is defined as [21]:

$$s^\gamma \approx \omega_h^\gamma \prod_{k=1}^{N} \frac{s+\omega_k'}{s+\omega_k} \ , \tag{19}$$

where $\omega_k' = \omega_b \omega_v^{(2k-1-\gamma)/N}$, $\omega_k = \omega_b \omega_v^{(2k-1+\gamma)/N}$, $\omega_v = \sqrt{\omega_h/\omega_b}$; In the above expressions, $[\omega_b, \omega_h]$ is the frequency range for which the approximation is designed to be valid; N is the order of the polynomial approximation; The term "generalized" implies that, in (19), N can be either even or odd [21], while the term "recursive" implies that the values of ω_k', ω_k result from a set of recursive equations [17]. The block diagram of ORA is shown in Fig. 2.

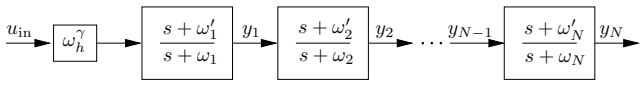

Fig. 2: Oustaloup's recursive approximation block diagram.

Figure 3 compares the theoretical frequency response of $s^{-0.7}$, which is given by (17) for $K = 1$, with the respective plots provided by ORAs of different dynamic orders. This simple example shows the typical behaviour of the ORA: the approximation is more accurate for higher dynamic orders and for frequencies closer to the middle of the interval $[\omega_b, \omega_h]$.

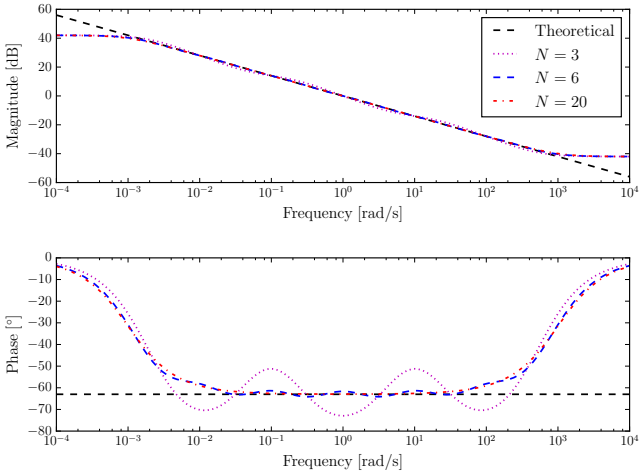

Fig. 3: Bode plot of the ORA for different approximation orders N ($\gamma = -0.7$; $[\omega_b, \omega_h] = [10^{-3}, 10^3]$ rad/s).

A final note on (19) is that the ORA of s^γ is typically accurate enough for fractional orders that satisfy $0 \leq |\gamma| \leq 1$. For higher fractional orders, accuracy can be maintained by implementing s^γ as a multiplication of a suitable integer order block and a fractional order block, as follows:

$$s^\gamma = s^n s^{\gamma-n}, \ n \in \mathbb{Z}, \ (\gamma - n) \in [0, 1] \ . \tag{20}$$

B. DAE Model

In time-domain, the ORA can be described by the following set of explicit DAEs:

$$\begin{aligned} \boldsymbol{\chi}_e{}' &= \boldsymbol{A}_e \boldsymbol{\chi}_e + \boldsymbol{B}_e u_{\text{in}} \\ 0 &= y_N - \boldsymbol{C}_e \boldsymbol{\chi}_e + \omega_h^\gamma u_{\text{in}} \ , \end{aligned} \tag{21}$$

where $\boldsymbol{\chi}_e = [\chi_{e,1} \ \ \chi_{e,2} \cdots \ \chi_{e,N}]^T$ is the ORA state vector;

$$\boldsymbol{A}_e = \begin{bmatrix} -\omega_1 & & & & \\ \omega_2' - \omega_2 & -\omega_2 & & & \\ \omega_3' - \omega_3 & \omega_3' - \omega_3 & -\omega_3 & & \\ \vdots & \vdots & \vdots & \ddots & \\ \omega_N' - \omega_N & \omega_N' - \omega_N & \cdots & \omega_N' - \omega_N & -\omega_N \end{bmatrix} ;$$

$$\boldsymbol{B}_e = \begin{bmatrix} \omega_h^\gamma(\omega_1' - \omega_1) & \omega_h^\gamma(\omega_2' - \omega_2) & \cdots & \omega_h^\gamma(\omega_N' - \omega_N) \end{bmatrix}^T ;$$

$$\boldsymbol{C}_e = \begin{bmatrix} 1 & 1 & \cdots & 1 \end{bmatrix}^T .$$

The dimensions of $\boldsymbol{A}_e$, $\boldsymbol{B}_e$, $\boldsymbol{C}_e$, are $N \times N$, $N \times 1$ and $1 \times N$, respectively. An alternative way to describe a dynamic model is by using a semi-implicit DAE formulation [27]. We propose the following, semi-implicit form of the ORA:

$$\begin{aligned} \chi_{s,1}' &= -\omega_1 \chi_{s,1} + \omega_h^\gamma u_{\text{in}} \\ \chi_{s,2}' - \chi_{s,1}' &= \omega_1' \chi_{s,1} - \omega_2 \chi_{s,2} \\ &\vdots \\ \chi_{s,N}' - \chi_{s,N-1}' &= \omega_{N-1}' \chi_{s,N-1} - \omega_N \chi_{s,N} \\ -\chi_{s,N}' &= \omega_N' \chi_{s,N} - y_N \ , \end{aligned}$$

where $\boldsymbol{\chi}_s = [\chi_{s,1} \ \ \chi_{s,2} \cdots \ \chi_{s,N}]^T$ is the ORA state vector; Using matrix notation, we have:

$$\boldsymbol{E}_s \boldsymbol{z}' = \boldsymbol{A}_s \boldsymbol{z} + \boldsymbol{B}_s u_{\text{in}} \ , \tag{22}$$

where $\boldsymbol{z} = [\boldsymbol{\chi}_s \ \ y_N]^T$ and

$$\boldsymbol{E}_s = \begin{bmatrix} 1 & & & & & \\ -1 & 1 & & & & \\ & \ddots & \ddots & & & \\ & & -1 & 1 & & \\ & & & -1 & 1 & \\ & & & & -1 & 0 \end{bmatrix} , \ \boldsymbol{B}_s = \begin{bmatrix} \omega_h^\gamma \\ 0 \\ \vdots \\ 0 \\ 0 \\ 0 \end{bmatrix} ,$$

$$\boldsymbol{A}_s = \begin{bmatrix} -\omega_1 & & & & & \\ \omega_1' & -\omega_2 & & & & \\ & \ddots & \ddots & & & \\ & & \omega_{N-2}' & -\omega_{N-1} & & \\ & & & \omega_{N-1}' & -\omega_N & \\ & & & & \omega_N' & -1 \end{bmatrix} ,$$

where the dimensions of $\boldsymbol{E}_s$, $\boldsymbol{A}_s$, $\boldsymbol{B}_s$, are $(N+1) \times (N+1)$, $(N+1) \times (N+1)$ and $(N+1) \times 1$, respectively. In (21), the total number of non-zero elements of the coefficient matrices is $\Theta(N^2)$, whereas in (22) it is $\Theta(N)$. Therefore, the proposed semi-implicit model is sparser than the explicit one. In addition, (22) prevents the input u_{in} to propagate through the equations to the output.

C. Steady State Error

Consider the simple FOC with transfer function $G_c(s) = Ks^\gamma$. By approximating s^γ from (19), we can write $G_c(s)$ as follows:

$$\begin{aligned} G_c(s) &\approx K\omega_h^\gamma \prod_{k=1}^{N} \frac{s+\omega_k'}{s+\omega_k} \\ &= \frac{c_1 s^N + c_2 s^{N-1} + \cdots + c_N}{d_1 s^N + d_2 s^{N-1} + \cdots + d_N} \ , \end{aligned} \tag{23}$$

with

$$c_N = K\omega_h^\gamma \prod_{k=1}^{N} \omega_k' K\omega_h^\gamma \omega_b^N \omega_v^{(N-\gamma)} \ , \qquad d_N = \prod_{k=1}^{N} \omega_k = \omega_b^N \omega_v^{(N+\gamma)} \ , \tag{24}$$

where we have substituted the expressions for ω_k and ω_k' as in (19) and $\sum_{k=1}^{N} = \frac{N(N+1)}{2}$. From (23), one can deduce that the controller's unity feedback closed-loop steady state error $e(t \to \infty)$ for an arbitrary input $R(s)$ is:

$$e(t\to\infty) = \lim_{s\to 0} \frac{sR(s)}{1+G_c(s)} = \frac{d_N}{c_N + d_N} \lim_{s\to 0} sR(s) = \frac{1}{K+\omega_b^\gamma} \lim_{s\to 0} sR(s) \ , \tag{25}$$

where we have substituted $\omega_v = \sqrt{\omega_h/\omega_b}$. The steady state error in (25) depends on K, ω_b^γ, and the applied input $R(s)$. Evaluating the controller's unit step input response yields $R(s) = 1/s$ and $e_{\text{step}}(t \to \infty) = 1/(K + \omega_b^\gamma)$. For $\gamma < 0$, we obtain that an ORA-based FO integral controller is not perfect tracking. This result is not consistent with the theoretical behaviour of Ks^γ, $\gamma < 0$, which has $e_{\text{step}}(t \to \infty) = 0$. However, the design of an almost perfect tracking FOC is possible with appropriate selection of ORA parameters.

D. Parameters Selection

While the value of N is usually constrained due to computational concerns, most studies that consider ORA-based FOCs in power systems provide a rather arbitrary selection of the range of frequencies $[\omega_b, \omega_h]$. This section discusses the tuning of ORA parameters and provides an empirical rule that simplifies the design of FOCs.

1) Low frequency ω_b: A very small ω_b reduces the steady state error in (25). However, a poor choice can significantly degrade the phase fitting of ORA. An example is shown in Fig. 4, where ω_b is varied from 10^{-3} to 10^{-8} rad/s.

2) High frequency ω_h: A very high ω_h may increase the system gain margin. Large gains lead to fast response and stability enhancement, as well as to elimination of steady state errors. However, increasing excessively the speed of the system response may trigger closed-loop resonant points. Note that such resonant points can remain undetected if they stem from unmodelled high frequency dynamics.

3) Approximation order N: The phase fitting degradation caused by the decrease of ω_b can be compensated by increasing the dynamic order N, e.g. from 7 to 11 (Fig. 4). Increasing N has an impact on the computational complexity, which can be a serious constraint, especially if multiple filters are required and if a large system (like real-world power systems) is studied. Another possible problem of a very high N is that multiple poles are placed very close to each other and close to the imaginary axis. For digital filters, such a pole-placement may affect the discretization process, with multiple poles being mapped on the unity circle, due e.g. to rounding errors.

Control parameters need to provide an adequate compromise among accuracy, computational burden and performance.

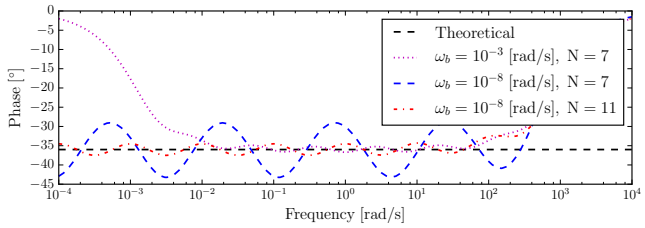

Fig. 4: Effect of ω_b on ORA frequency response. ($\gamma = -0.4$; $\omega_h = 10^3$ rad/s).

A good practice is to limit the range of $[\omega_b, \omega_h]$ to the frequencies of the dynamics of interest. This also avoids unexpected resonances, as discussed above. Then, given a range $\omega_b = 10^{-\mu_b}$ and $\omega_h = 10^{\mu_h}$, $\mu_b, \mu_h \geq 0$, a choice that provides a very good compromise is $N = \mu_b + \mu_h$, with $N \geq 4$.

V. Case Study I: WSCC 9-bus system

This section presents three power system applications of FOCs. First, we discuss a FO integral controller for secondary frequency regulation. Then, we study a FO lead-lag controller for primary frequency regulation of an ESS. Finally, we examine the performance of voltage regulation provided by a STATCOM which comprises multiple FOPI controllers. In all three examples, the pre-disturbance equilibrium of the fractional DAE model is stable, i.e. condition (16) holds. That said, the focus is on time-domain simulations carried to discuss the dynamic performance of ORA-based FOCs and check the system stability under large disturbances. Examples of this section are based on the WSCC 9-bus system. In the remainder of the paper, all simulation results are obtained with Dome [28].

A. Automatic Generation Control

In this example, an AGC that coordinates the three generators and provides secondary frequency regulation is included in the WSCC system. The AGC measures the Center-of-Inertia (COI) frequency (ω_{coi}) and produces a dynamic active power signal (p_{s}), which is sent to the synchronous generator turbine governors, and is proportional to their droops. The power order ($p_{\text{ord},i}$) received by the i-th governor is:

$$p_{\text{ord},i} = \frac{R_i}{R_T} p_{\text{s}} \ , \qquad i = \{1,2,3\} \ , \tag{26}$$

where R_i is the i-th TG droop constant; and $R_T = R_1 + R_2 + R_3$. The simplest model of an AGC assumes an integral controller. The differential equation that describes the dynamic behaviour of a FO Integral (FOI) AGC is:

$$p_{\text{s}}^{(\gamma)} = K_i(\omega^{\text{ref}} - \omega_{\text{coi}}) \ , \tag{27}$$

where K_i is the FOI-AGC gain; ω^{ref} is the reference angular frequency; and γ is the order of integration. The IO version of this controller (I-AGC) is obtained for $\gamma = 1$.

We compare the performance of the I-AGC and the ORA-based FOI-AGC. With this aim, a three-phase fault is considered at bus 4 occurring at $t = 3$ s. After 80 ms, the line

that connects buses 4 and 5 trips and the fault is cleared. The parameters of both controllers are tuned by optimizing the COI frequency profile through trial-and-error. The I-AGC gain is $K_i = 15$, while the parameters of the FOI-AGC are $K_i = 50$ and $\gamma = 0.7$. Regarding the ORA parameters, taking into account the discussion in IV-D, we set $[\omega_b, \omega_h] = [10^{-3}, 10^{1}]$ rad/s, $N = 4$. Figure 5 presents the COI frequency response of the system without AGC; with I-AGC; with FOI-AGC. The FOI-AGC improves significantly the dynamic response of the frequency of the system. Note that, with the selected parameters, the FOI-AGC achieves practically a perfect tracking.

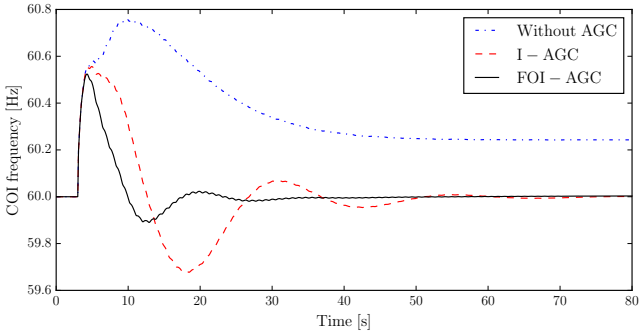

Fig. 5: WSCC system with AGC: COI frequency.

B. Energy Storage System

In this example, we assume that a converter-interfaced ESS is installed at bus 6 of the 9-bus system. A simplified model is employed to describe the ESS dynamics. Figure 6 shows the block diagram of the ESS active power control. The ESS measures the local frequency at bus 6 and regulates its active power p_{ESS} to provide frequency support. The frequency error $\omega_6^{\text{ref}} - \omega_6$ is filtered. $T_{\text{f},p}$ is the time constant of the applied filter and $x_{\text{f},p}$ is the filtered signal as well as the input of the frequency control $G(s)$. Finally, $T_{\text{ESS},p}$ is the time constant of the ESS active power dynamics. The interested reader can find more details on the employed ESS model in [29].

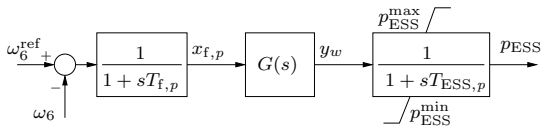

Fig. 6: Active power flow of simplified ESS model.

In this example, $G(s)$ is assumed to be a FO lead-lag with transfer function $K(T_1 s^\gamma + 1)/(T_2 s^\gamma + 1)$. The equations that describe the FO lead-lag are:

$$\begin{aligned} T_2 x_w^{(\gamma)} &= K x_{\text{f},p} - x_w \ , \\ y_w &= x_w + T_1 x_w^{(\gamma)} \ , \end{aligned} \tag{28}$$

where x_w is the controller's state. The IO version of this controller (IO lead-lag) is obtained for $\gamma = 1$.

We consider the same disturbance examined at the previous example (fault at bus 4 cleared after 80 ms). Two implementations of the IO lead-lag are compared, namely, the IO lead-lag and the ORA-based IO lead-lag controller for $\gamma = 1$, $[\omega_b, \omega_h] = [10^{-4}, 10^{4}]$ rad/s. The results are shown in Fig. 7. The value $\omega_h = 10^4$ rad/s is high enough to trigger a closed-loop high frequency resonant point, which significantly impacts the control output. Figure 7 also shows that, while it is independent from the approximation order, the overshoot can be avoided by properly reducing the value of ω_h.

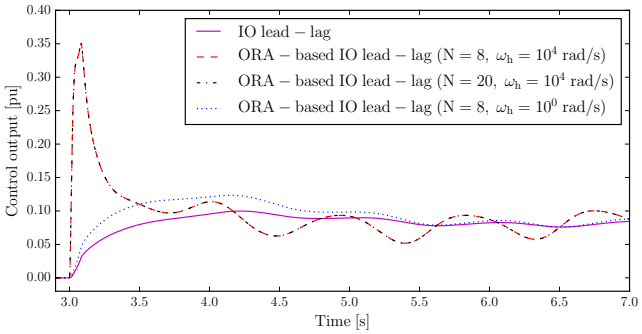

Fig. 7: WSCC system with ESS frequency control: lead-lag parameters: $T_1 = 2$ s, $T_2 = 0.01$ s, $K = 10$; ORA parameters: $\omega_b = 10^{-4}$ rad/s, $\gamma = 1$.

Next, the dynamic performance of the IO lead-lag is compared with two ORA-based FO lead-lags, namely FOLL1 and FOLL2, which have different tuning. The parameters of the three controllers are shown in Table I. For comparison, the gain and time constants of FOLL1 have been set equal to the ones of the IO lead-lag. In this case, only the order γ needs to be tuned. In general, however, the control parameters of a FOC are not directly mapped onto those of its IO version and should be retuned. FOLL2 represents the retuned controller. To tune FOLL2, $T_1 = 2$ s is fixed and the rest of the parameters are selected by optimizing the local bus frequency profile through trial-and-error. The response of the frequency at bus 6 is shown in Fig. 8. Shifting the fractional order γ (FOLL1) allows reducing both the frequency overshoot and the steady state error of the local bus frequency. Retuning all control parameters leads to a further performance improvement (FOLL2).

TABLE I: Parameters of the ESS lead-lag frequency controllers.

IO lead-lag	$T_1 = 2$ s, $T_2 = 0.01$ s, $K = 20$,
FOLL1	$T_1 = 2$ s, $T_2 = 0.01$ s, $K = 20$, $\gamma = 0.3$
FOLL2	$T_1 = 2$ s, $T_2 = 0.005$ s, $K = 60$, $\gamma = 0.2$

C. STATCOM

In this example, a STATCOM connected to bus 8 provides reactive power support. The reactive power variations provided by the STATCOM rely on the control of a Voltage Source Converter (VSC). The VSC is represented by an average value model. It consists of an AC/DC converter, an AC-side high voltage/medium voltage transformer, and a DC-side condenser. The VSC parameters are given in [30].

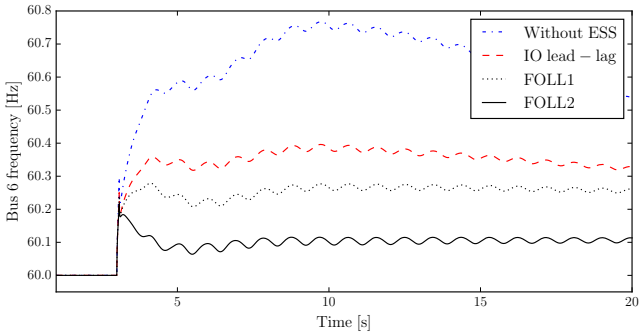

Fig. 8: WSCC system with ESS frequency control: ORA parameters: $[\omega_b, \omega_h] = [10^{-3}, 10^{1}]$ rad/s, $N = 4$.

The VSC is controlled by employing a vector-current control strategy. The control is based on a dq-axis reference frame and a phase-locked loop refers all phases to the AC side voltage phasor angle [31]. The block diagram of the considered vector-current control is depicted in Fig. 9. The d- and q- axis current components are decoupled by the inner control loop, through the controllers $G_{\mathrm{i},d}(s)$ and $G_{\mathrm{i},q}(s)$, respectively. In the STATCOM configuration, the outer control loop utilizes the d- and q- axis current components to provide regulation of the DC and AC voltages, through the controllers $G_{\mathrm{o},d}(s)$ and $G_{\mathrm{o},q}(s)$, respectively.

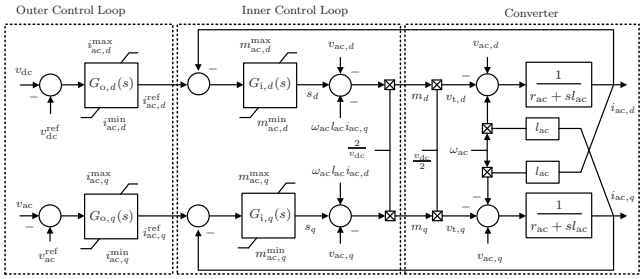

Fig. 9: VSC converter, outer and inner control in dq-frame.

$G_{\mathrm{i},d}(s)$, $G_{\mathrm{i},q}(s)$, $G_{\mathrm{o},d}(s)$ and $G_{\mathrm{o},q}(s)$, are assumed to be FO Proportional-Integral (FOPI) controllers. The equations that describe the behaviour of the FOPI are:

$$\begin{aligned} x_G^{(\gamma)} &= K_i u_G \ , \\ y_G &= K_p u_G + x_G \ , \end{aligned} \tag{29}$$

where K_p and K_i, are the proportional and integral gains, respectively; x_G, y_G, are the state and output variable of the controller, respectively; and u_G is the controller input. The IO version of this controller (IOPI) is obtained for $\gamma = 1$.

To study the impact of the STATCOM voltage regulation, we consider a stressed operating condition of the WSCC system. With this aim, the consumed power is increased by 60% compared to the base case. Then, for the purpose of transient analysis, an additional 15% consumption increase of the load connected at bus 8 is considered, occurring at $t = 3$ s. The system response is compared for the three following scenarios: without the STATCOM; with the STATCOM connected and all four controllers modelled as IOPIs; with the STATCOM and the four controllers modelled as ORA-based FOPIs. The values of the STATCOM control parameters are shown in Table II. The inner control loop parameters are tuned based on the pole cancellation technique as in [32], while the outer control loop parameters are tuned by optimizing the local bus voltage profile though trial-and-error. Regarding the FOPIs ORA parameters, we have set the frequency range at $[10^{-3}, 10^{2}]$ rad/s for the inner control loop; at $[10^{-4}, 10^{1}]$ rad/s for the outer control loop. The dynamic order is $N = 5$ for all FOPI controllers.

TABLE II: Parameters of the STATCOM controllers.

	IOPIs		FOPIs		
	K_p	K_i	K_p	K_i	γ
$G_{\mathrm{i},d}(s)$	0.2	20	0.2	20	0.20
$G_{\mathrm{i},q}(s)$	0.2	20	0.2	20	0.25
$G_{\mathrm{o},d}(s)$	50	25	50	25	0.40
$G_{\mathrm{o},q}(s)$	2.3	6	2.3	80	0.50

Simulation results are presented in Fig. 10. The use of multiple FOPIs for STATCOM voltage regulation is able to provide a significant improvement to the local voltage response.

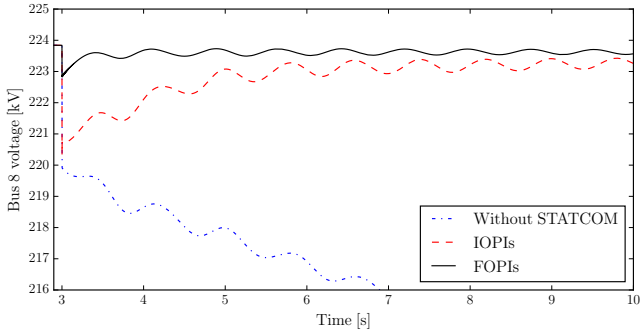

Fig. 10: WSCC system with STATCOM: voltage at bus 8.

VI. Case Study II: All-Island Irish System

In this section we present results on a detailed model of the all-island Irish transmission system. Static data of the Irish network are provided by the transmission system operator, EirGrid Group. Dynamic data are determined based on current knowledge of generator capacities and technologies. The system consists of 1,479 buses; 1,851 transmission lines and transformers; 245 loads; 22 synchronous generators with primary voltage, frequency controllers; 6 PSSs; 173 wind generators; and an I-AGC.

The Irish system model has been validated by utilizing the frequency data from a severe event that occurred in the real system [33]. The examined event refers to the tripping – on the 28-th of February 2018 – of the VSC-HVDC link East-West Inter-connector (EWIC) that connects the Irish and the Great Britain transmission systems. At that moment, Ireland was exporting 470 MW to Great Britain. Following the loss of the EWIC, the frequency in the Irish grid showed

a peak of 50.42 Hz, which led to the triggering of over-frequency protections and wind farm active power generation curtailment.

A comparison of the actual system response and the one simulated with Dome is shown in in Fig. 11. As it can be seen, the simulated transient closely follows the real system behaviour.

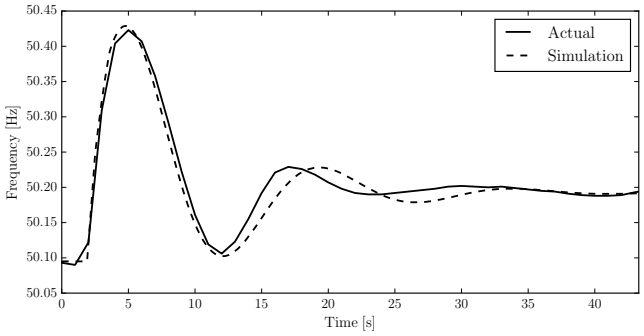

Fig. 11: Irish system: Frequency response following the loss of EWIC.

We examine the impact of FOC on the secondary frequency regulation of the system. To this aim, we substitute the I-AGC with the FOI-AGC model described by (27). The parameters of the FOI-AGC are tuned to $K_i = 500$, $\gamma = 0.15$. The ORA parameters are $[\omega_b, \omega_h] = [10^{-3}, 10^{1}]$ rad/s, $N = 4$. Figure 12 shows the frequency response of the system with I-AGC and FOI-AGC. As it can be seen, the FOI-AGC is able to improve the frequency regulation of the Irish system.

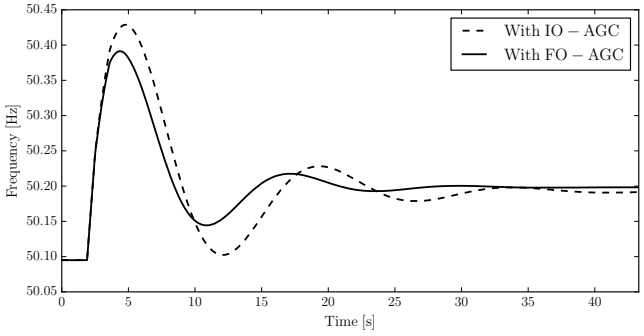

Fig. 12: Irish system: Impact of FO-AGC on frequency response.

VII. Conclusions

The paper studies the theory, stability analysis, computer implementation and practical design aspects of FOCs for power system applications. The paper provides a comprehensive theory on fractional calculus for control, as well as a detailed description of ORA-based FOCs. In all considered examples, the proposed FOCs are shown to perform better than the conventional IO versions while requiring only a little additional tuning effort. This is a general result that shows the potential of FOCs for power system applications.

We will dedicate future work to examine the impact of control saturation limits on ORA-based FOCs performance.

References

[1] G. W. Leibniz, "Letter from Hanover, Germany, September 30, 1695 to G. A. L'Hospital," *Leibnizen Mathemutische Schriften*, vol. 2, no. 1, pp. 301–302, Olms Verlag., Hildesheim, Germany, 1962. Published in 1849.

[2] J. Liouville, "Mémoire sur quelques Quéstions de Géometrie et de Mécanique, et sur un nouveau genre de Calcul pour résoudre ces Quéstions," *Journ. Ecole Polytech.*, vol. 13, pp. 1–69, 1832, Sect. 21.

[3] H. Bode, *Network Analysis and Feedback Amplifier Design*. Princeton, NJ: Van Nostrand, 1945.

[4] A. Oustaloup, *La commande CRONE (commande robuste d'ordre non entier)*. Hermés, Paris, 1991.

[5] I. Podlubny, "Fractional-order systems and $PI^{\lambda}D^{\mu}$-controllers," *IEEE Trans. Autom. Control*, vol. 44, no. 1, pp. 208–214, Jan. 1999.

[6] ——, *Fractional differential equations, volume 198: an introduction to fractional derivatives, fractional differential equations, to methods of their solution and some of their applications*. Academic Press, 1999.

[7] I. S. Jesus and J. A. T. Machado, "Fractional control of heat diffusion systems," *Nonlinear Dyn.*, vol. 54, no. 3, pp. 263–282, Nov. 2008.

[8] M. Lazarević, "Finite time stability analysis of PD^{α} fractional control of robotic time-delay systems," *Mech. Res. Comm.*, vol. 33, no. 2, pp. 269 – 279, Mar. 2006.

[9] M. Zamani, M. Karimi-Ghartemani, N. Sadati, and M. Parniani, "Design of a fractional order PID controller for an AVR using particle swarm optimization," *Control Eng. Practice*, vol. 17, no. 12, pp. 1380 – 1387, Dec. 2009.

[10] Y. Tang, M. Cui, C. Hua, L. Li, and Y. Yang, "Optimum design of fractional order $pi^{\lambda}d^{\mu}$ controller for avr system using chaotic ant swarm," *Expert Syst. with Applications,*, vol. 39, no. 8, pp. 6887–6896, 2012.

[11] I. Pan and S. Das, "Frequency domain design of fractional order PID controller for AVR system using chaotic multi-objective optimization," *Int. Journ. of Electr. Power Energy Syst.*, vol. 51, pp. 106 – 118, Oct. 2013.

[12] S. A. Taher, M. H. Fini, and S. F. Aliabadi, "Fractional order PID controller design for LFC in electric power systems using imperialist competitive algorithm," *Ain Shams Eng. Journ.*, vol. 5, no. 1, pp. 121 – 135, Mar. 2014.

[13] S. Saxena, "Load frequency control strategy via fractional-order controller and reduced-order modeling," *Int. Journ. Electr. Power Energy Syst.*, vol. 104, pp. 603 – 614, Jan. 2019.

[14] L. Chaib, A. Choucha, and S. Arif, "Optimal design and tuning of novel fractional order PID power system stabilizer using a new metaheuristic Bat algorithm," *Ain Shams Eng. Journ.*, vol. 8, no. 2, pp. 113 – 125, Jun. 2017.

[15] M. B. Delghavi, S. Shoja-Majidabad, and A. Yazdani, "Fractional-order sliding-mode control of islanded distributed energy resource systems," *IEEE Trans. Sust. Energy*, vol. 7, no. 4, pp. 1482–1491, Oct. 2016.

[16] B. M. Vinagre, I. Podlubny, and V. Feliu, "Some approximations of fractional order operators used in control theory and applications," *Journ. of Fract. Calc. Appl. Anal.*, pp. 231–248, Jan. 2000.

[17] A. Oustaloup, F. Levron, B. Mathieu, and F. M. Nanot, "Frequency-band complex noninteger differentiator: characterization and synthesis," *IEEE Trans. Circ. Syst. I: Fund. Theory Appl.*, vol. 47, no. 1, pp. 25–39, Jan. 2000.

[18] A. Oustaloup, P. Melchior, P. Lanusse, O. Cois, and F. Dancla, "The CRONE toolbox for Matlab," *CACSD. Conf. Procs IEEE Int. Symposium on Computer-Aided Control Syst. Design*, pp. 190–195, Sep. 2000.

[19] D. Valério and J. Costa, "Ninteger: a non-integer control toolbox for Matlab," *Procs of the 1st IFAC Workshop on Fract. Differ. Appl.*, Jan. 2004.

[20] A. Tepljakov, E. Petlenkov, and J. Belikov, "FOMCON: Fractional-order modeling and control toolbox for Matlab," *Procs of the 18th Int. Conf. Mixed Design of Integrated Circ. Syst.-MIXDES*, Jun. 2011.

[21] C. A. Monje, Y. Chen, B. M. Vinagre, D. Xue, and V. Feliu, *Fractional-order Systems and Controls, Fundamentals and Applications*. Springer, 2010.

[22] M. Caputo and M. Fabrizio, "A new definition of fractional derivative without singular kernel," *Progr. Fract. Differ. Appl.*, vol. 1, no. 2, pp. 73–85, Apr. 2015.

[23] A. Atangana and D. Baleanu, "New fractional derivatives with nonlocal and non-singular kernel: Theory and application to heat transfer model," *Therm. Sci.*, vol. 20, no. 2, pp. 763–769, Jan. 2016.

[24] C. Li and W. Deng, "Remarks on fractional derivatives," *Applied Mathematics and Comput.*, vol. 187, no. 2, pp. 777 – 784, Apr. 2007.

[25] I. Pétras, "Stability of fractional-order systems with rational orders: A survey," *Fract. Calc. Appl. Anal.*, vol. 12, no. 3, 2009.

[26] P. M. Anderson and A. A. Fouad, *Power system control and stability*, 2nd ed. IEEE Press: Wiley-Interscience, 2003, previous ed.: Ames: Iowa State University Press, 1977.
[27] F. Milano, "Semi-implicit formulation of differential-algebraic equations for transient stability analysis," *IEEE Trans. Power Syst.*, vol. 31, no. 6, pp. 4534–4543, Nov. 2016.
[28] ——, "A Python-based software tool for power system analysis," in *Procs of the IEEE PES General Meeting*, Jul. 2013.
[29] F. Milano and Á. Ortega Manjavacas, *Converter-Interfaced Energy Storage Systems: Context, Modelling and Dynamic Analysis*. Cambridge University Press, 2019.
[30] M. A. A. Murad, Á. Ortega, and F. Milano, "Impact on power system dynamics of PI control limiters of VSC-based devices," *Procs of the Power Syst. Comput. Conf. (PSCC)*, pp. 1–7, Jun. 2018.
[31] Y. Amirnaser and I. Reza, *Voltage-sourced converters in power systems: modeling, control, and applications*. Wiley-IEEE Press, 2012.
[32] M. A. A. Murad and F. Milano, "Modeling and simulation of pi-controllers limiters for the dynamic analysis of vsc-based devices," *IEEE Trans. Power Syst.*, vol. 34, no. 5, pp. 3921–3930, Sep. 2019.
[33] M. A. A. Murad, G. Tzounas, M. Liu, and F. Milano, "Frequency control through voltage regulation of power system using svc devices," in *2019 IEEE Power Energy Society General Meeting*, Aug. 2019.

Georgios Tzounas (S'17) received from the National Technical University of Athens, Greece, the ME in Electrical and Computer Engineering in 2017. Since September 2017, he is Ph.D. candidate with Univ. College Dublin, Ireland. His scholarship is funded through the SFI Investigator Award with title "Advanced Modelling for Power System Analysis and Simulation" (AMPSAS). His current research interests include stability analysis and robust control of power systems.

Ioannis Dassios received his Ph.D. in Applied Mathematics from the Dpt of Mathematics, Univ. of Athens, Greece, in 2013. He worked as a Postdoctoral Research and Teaching Fellow in Optimization at the School of Mathematics, Univ. of Edinburgh, UK. He also worked as a Research Associate at the Modelling and Simulation Centre, University of Manchester, UK, and as a Research Fellow at MACSI, Univ. of Limerick, Ireland. He is currently a UCD Research Fellow at UCD, Ireland.

Mohammed Ahsan Adib Murad (S'18) received B.Sc. degree in electrical engineering from Islamic University of Technology, Bangladesh in 2009, and double M.Sc. degree in Smart Electrical Networks and Systems from KU Leuven, Belgium and KTH, Sweden in 2015. He is currently pursuing the Ph.D. degree with the Dpt of Electrical and Electronic Engineering, University College Dublin, Ireland. His current research interests include power system modelling and dynamic analysis.

Federico Milano (S'02, M'04, SM'09, F'16) received from the Univ. of Genoa, Italy, the ME and Ph.D. in Electrical Eng. in 1999 and 2003, respectively. From 2001 to 2002 he was with the Univ. of Waterloo, Canada, as a Visiting Scholar. From 2003 to 2013, he was with the Univ. of Castilla-La Mancha, Spain. In 2013, he joined the Univ. College Dublin, Ireland, where he is currently Professor of Power Systems Control and Protections. His research interests include power system modelling, control and stability analysis.